Congresso de Métodos Numéricos em Engenharia 2015
Lisboa, 29 de Junho a 2 de Julho, 2015

THERMAL GRADIENTS PREDICTION IN THE GLEEBLE SYSTEM USING A 3D FINITE ELEMENT MODEL

J.M.P. Martins[1]*, J.L. Alves[2], D.M. Neto[1], M.C. Oliveira[1] and L.F. Menezes[1]

1: CEMUC, Department of Mechanical Engineering
University of Coimbra
Polo II, Pinhal de Marrocos, 3030-788 Coimbra, Portugal
e-mail: {joao.pmartins, diogo.neto, marta.oliveira, luis.menezes}@dem.uc.pt

2: MEMS, Microelectromechanical Systems Research Unit
University of Minho
Campus de Azurém, 4800-058 Guimarães, Portugal
e-mail: jlalves@dem.uminho.pt

Keywords: Gleeble testing machine, Direct resistance heating, Thermal gradients, Finite element method

Abstract *This study present a 3D finite element model able to predict the axial temperature gradients on a tensile specimen, which is heated by the direct resistance system used on a Gleeble system. A new algorithm is proposed to control the heat generation rate required to simulate the metal heating by direct resistance. The predicted temperature distribution was compared with data recorded experimentally along the specimen. The results shown that the algorithm developed can be a good solution for the temperature prediction on the specimen under the specified conditions.*

1. INTRODUCTION

The automotive industry has made significant efforts in recent years to reduce the fuel consumption in passenger cars and consequently reduce the carbon dioxide (CO2) emissions rates to fulfil the new environmental demands [1]. The adoption of light-weight materials, such as aluminium [2] and magnesium alloys [3], allows the weight reduction in body-in-white. Nevertheless, the formability of these alloys at room temperature is considerably low when compared with low carbon steels, which limits its widespread application [4]. Indeed, the formability can be significantly improved by warm forming, since the increase of temperature leads to a decrease in the material flow stress and improves the ductility [5].

Typically the warm sheet metal forming process of light-weight alloys is performed in the temperature range of 200ºC to 350ºC. The behaviour of two Al–Mg–Si alloys during drawing was investigated by Ghosh et al. [6] at room and warm temperatures, concluding that the force–displacement evolution is strongly influenced by the blank temperature. Moreover, the formability (limiting drawing ratio) and ductility of these alloys is enhanced by the warm

temperatures, as illustrated by Abedrabbo et al. [7]. Another advantage of warm forming processes is the decrease of the springback effects, resulting from the change of the stress state in the formed sheet after forming [8]. Besides, the stretcher lines arising in the AA5xxx series (Al–Mg alloys), due to the Portevin–Le Chatelier (PLC) effect, vanish at warm temperatures, as highlighted in the experimental study performed by Coër et al. [9].
The mechanical behaviour of the metallic sheets at warm temperatures needs to be studied to develop adequate constitutive models. The Gleeble thermo-mechanical testing system has become a standard machine for these type of studies, since it combines accurate high heating rates, while guaranteeing an homogeneous and constant temperature in a small zone of the samples [10], [11]. This is only possible due to the direct resistance system used on the Gleeble testing machine. This system involves an electrical current induced in the specimen using a power source, which heats the specimen by Joule’s effect due to the material’s resistivity.
Several numerical models have been developed to predict the temperature distribution, which resort to electro-thermal formulations [10], [12], [13]. This study presents a novel 3D finite element (FE) model to predict the temperature distribution on the specimen heated by the Gleeble direct resistance system. The developed FE model avoids the difficulties inherent to an electro-thermal coupling being based on classical thermal transient FE model. The numerical results are compared with experimental ones, which are obtained from a tensile specimen heated on a Gleeble 3,500 system.

2. EXPERIMENTAL SET-UP

The experimental results presented in this study were obtained by Coër et al.[11] and are used to validate the developed finite element model. In the experimental tensile test, a specimen was heated on a Gleeble 3,500 system and the temperature evolution was recorded in four points. The experimental set-up used can be observed in Figure 1(a).

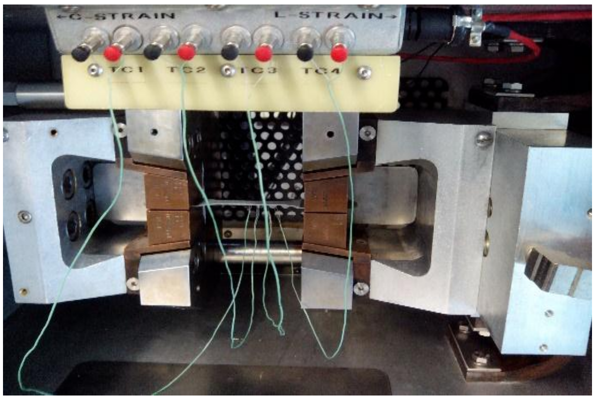

(a)

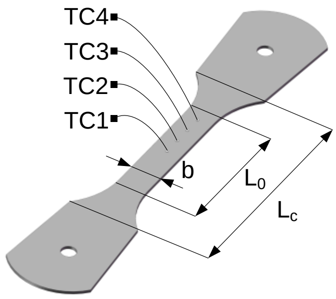

(b)

Figure 1. Gleeble testing system: (a) experimental set-up and (b) geometry of the specimen ($L_0 = 40mm$, $b = 10mm$ and $L_c = 80mm$).

Throughout the heating stage, the specimen was clamped with cooper grips, which were water cooled, forcing an axial thermal gradient on the specimen. Thus, only the centre of the specimen was at the prescribed temperature (200ºC) after the prescribed time of 13.4s. The temperature on the specimen was measured with four thermocouples, which were previously welded on the surface of the specimen equally spaced (6 mm) along the specimen axis (Figure 1(b)). The thermocouple TC1 provides the actual temperature of the specimen at its centre point. This information is used by the Gleeble control system, which is compared with the prescribed heating rate in each time instant. Thus, the electric current applied is calculated to ensure the prescribed heating rate.
The environment temperature and the initial temperature of the specimen was about 22ºC. The geometry of the specimen used is shown in Figure 1(b). The material considered for this work was an automotive sheet: AA5754-O aluminium alloy sheet with 1 mm of thickness. The thermal properties for the aluminium alloy and for the cooper grips are presented in Table 1.

Sepcimen Material	AA5754-O
Density (kg/m^3)	2700
Specific heat (J/kg/°C)	900
Conductivity (W/m/°C)	220
Grips material	Copper
Density (kg/m^3)	8800
Specific heat (J/kg/°C)	400
Conductivity (W/m/°C)	300

Table 1. Thermal properties of the specimen and grips materials [8], [14].

3. FINITE ELEMENT MODEL

The heat equation combined with the Fourier's law of conduction applied to a continuous medium, with arbitrary volume $\left(V \in \mathbb{R}^3\right)$ bounded by a closed surface S, can be expressed as follows:

$$\rho c \frac{\partial T}{\partial t} = \mathbf{k} \, \mathrm{grad}(T) + \dot{q}, \tag{1}$$

where ρ and c represent the specific mass and the specific heat of the continuous medium, respectively. $\mathbf{k}$ is the conductivity tensor and $\dot{q}$ is the energy rate generation per unit of volume.
The classical boundary heat exchange conditions comprise the heat transfer modes of convection and radiation. To model the convection boundary condition it is necessary to know the convection coefficient h_c and the exterior temperature T_∞ in order to define the convection heat flux as follows:

$$q_{\mathrm{conv}} = h_{\mathrm{c}}\left(T - T_{\infty}\right), \tag{2}$$

The radiation boundary condition term is defined also based on a heat flux:

$$q_{\mathrm{rad}} = h_{\mathrm{r}}\left(T - T_{\mathrm{sur}}\right), \tag{3}$$

in which the h_r is defined by:

$$h_{\mathrm{r}} = \varepsilon\sigma\left(T^2 + T_{\mathrm{sur}}^2\right)\left(T + T_{\mathrm{sur}}\right), \tag{4}$$

where T_{sur} is the surrounding temperature, ε is the emissivity of the surface and σ is the Stefan–Boltzmann constant.

The weak form of Eq. (1) can be written in matrix form as:

$$\mathbf{C}\dot{\mathbf{T}} + \left(\mathbf{K}_{\mathrm{cond}} + \mathbf{K}_{\mathrm{conv/rad}}\right)\mathbf{T} = \mathbf{Q} + \mathbf{f} \tag{5}$$

where $\mathbf{C}$ is the thermal capacity matrix and, $\mathbf{K}_{\mathrm{cond}}$ and $\mathbf{K}_{\mathrm{conv/rad}}$ are the conductivity and the convection/radiation stiffness matrices, respectively. $\mathbf{Q}$ and $\mathbf{f}$ are the vectors of heat generation and heat fluxes on the surface, respectively. These matrices and vectors can be expressed as:

$$\mathbf{C} = \int_V \mathbf{N}^{\mathrm{T}} \rho c \mathbf{N} dV \tag{6}$$

$$\mathbf{K}_{\mathrm{cond}} = \int_V \mathbf{M}^{\mathrm{T}} \mathbf{k} \mathbf{M} dV \tag{7}$$

$$\mathbf{K}_{\mathrm{conv/rad}} = \int_S \mathbf{N}_{\mathrm{s}}^{\mathrm{T}} h_{\mathrm{conv}} \mathbf{N}_{\mathrm{s}} dS + \int_S \mathbf{N}_{\mathrm{s}}^{\mathrm{T}} h_{\mathrm{r}} \mathbf{N}_{\mathrm{s}} dS \tag{8}$$

$$\mathbf{Q} = \int_V \mathbf{N}^{\mathrm{T}} \dot{q} dV \tag{9}$$

$$\mathbf{f} = \int_S \mathbf{N}_{\mathrm{s}}^{\mathrm{T}} h_{\mathrm{conv}} \mathbf{T}_{\infty} dS + \int_S \mathbf{N}_{\mathrm{s}}^{\mathrm{T}} h_{\mathrm{r}} \mathbf{T}_{\mathrm{r}} dS \tag{10}$$

where $\mathbf{N}(x)$ and $\mathbf{N}_{\mathrm{s}}(x)$ are matrices containing the shape functions associated with the volume and the surface of the body, respectively. Also, $\mathbf{M} = \mathrm{grad}(\mathbf{N})$.

In transient heat conduction analysis, Eq. (4) must be integrated over the time. Different time integration methods based in one or more time steps can be adopted [15]. The generalized trapezoidal method is used in this study [16]. This time integration method can be deduced from the Taylor's expansion, by neglecting the second and higher-orders terms and introducing a time weighting factor α, varying between 0 and 1. Thus, the temperature field at instant $t + \Delta t$ is obtained using the following equation:

$$\mathbf{T}_{t+\Delta t} = \mathbf{T}_t + \left[\alpha \dot{\mathbf{T}}_{t+\Delta t} + \left(1-\alpha\right)\dot{\mathbf{T}}_t\right]\Delta t. \tag{11}$$

where Δt is the incremental time. Applying the definition of the trapezoidal method into Eq. (4), the following expression is obtained:

$$\left[\frac{1}{\Delta t}\mathbf{C}+\alpha\left(\mathbf{K}_{\text{cond}}+\mathbf{K}_{\text{conv/rad}}\right)\right]\mathbf{T}_{t+\Delta t}-\left[\frac{1}{\Delta t}\mathbf{C}-\left(1-\alpha\right)\left(\mathbf{K}_{\text{cond}}+\mathbf{K}_{\text{conv/rad}}\right)\right]\mathbf{T}_{t}= \\ \left(1-\alpha\right)\mathbf{Q}_{t}+\alpha\mathbf{Q}_{t+\Delta t}+\left(1-\alpha\right)\mathbf{f}_{t}+\alpha\mathbf{f}_{t+\Delta t}. \tag{12}$$

Depending on the value selected for α, the generalized trapezoidal method reduces to time integration methods well-known such as, $\left(\alpha=0\right)$ Euler forward method, $\left(\alpha=\frac{1}{2}\right)$ Crank Nickolson method, $\left(\alpha=\frac{2}{3}\right)$ Galerkin method and $\left(\alpha=1\right)$ Euler backward method [17].

Only the Euler backward is known to be unconditionally stable for non-linear thermal problems [18], i.e. starting from a thermal equilibrium state at time t, it reaches a thermal equilibrium state at time $t+\Delta t$. The application of the Newton–Raphson iterative scheme to the Euler backward method results in the following linearized system of equations:

$$\left(\frac{1}{\Delta t}\mathbf{C}_{t+\Delta t}^{i}+\mathbf{K}_{t+\Delta t}^{i}\right)\Delta\mathbf{T}_{t+\Delta t}^{i+1}=\left(\frac{1}{\Delta t}\mathbf{C}_{t+\Delta t}^{i}\right)\mathbf{T}_{t}+\mathbf{Q}_{t+\Delta t}^{i}+\mathbf{f}_{t+\Delta t}^{i}-\left(\frac{1}{\Delta t}\mathbf{C}_{t+\Delta t}^{i}+\mathbf{K}_{t+\Delta t}^{i}\right)\mathbf{T}_{t+\Delta t}^{i}, \tag{13}$$

where the superscript i and the subscript t, which follow the vectors and matrices, represent the iteration number and the configuration where the vectors and matrices are calculated, respectively. The matrix $\mathbf{K}$ is given by:

$$\mathbf{K}=\mathbf{K}_{\text{cond}}+\mathbf{K}_{\text{conv/rad}}. \tag{14}$$

The adoption of a fully implicit method (Newton–Raphson) presents the drawback of excessive computational cost, contrasting with explicit and semi-implicit methods such as Euler's method, Crank Nickolson's method and Galerkin's method. However, implicit algorithms guarantee the equilibrium in all increments, leading to stable results. It is recognized that most of the time spent by fully implicit methods is related with the iterative cycle [19]. Nevertheless, the computation time of the implicit method can be reduced using an initial guess close to the solution. Therefore a prediction/correction algorithm type is adopted in this work to solve the non-linear heat problem. In the prediction phase, an explicit/semi-implicit algorithm $\left(\alpha<1\right)$ is used to solve the thermal problem combined with an r_{min}-strategy to control the size of the time increment [20], [21]. The obtained solution is used as initial guess for the correction phase $\left(\alpha=1\right)$.

3.1. Gleeble heating system

The thermal FE model aims to simulate the heating stage that occurs in the tests performed on Gleeble machine, described in section 2. In this context, due to geometric and material symmetry conditions (Figure 1), only one eighth of the model was considered. The tensile specimen and the copper grips were discretized as a single body using isoparametric 8-node linear hexahedral finite elements, as shown in Figure 2.

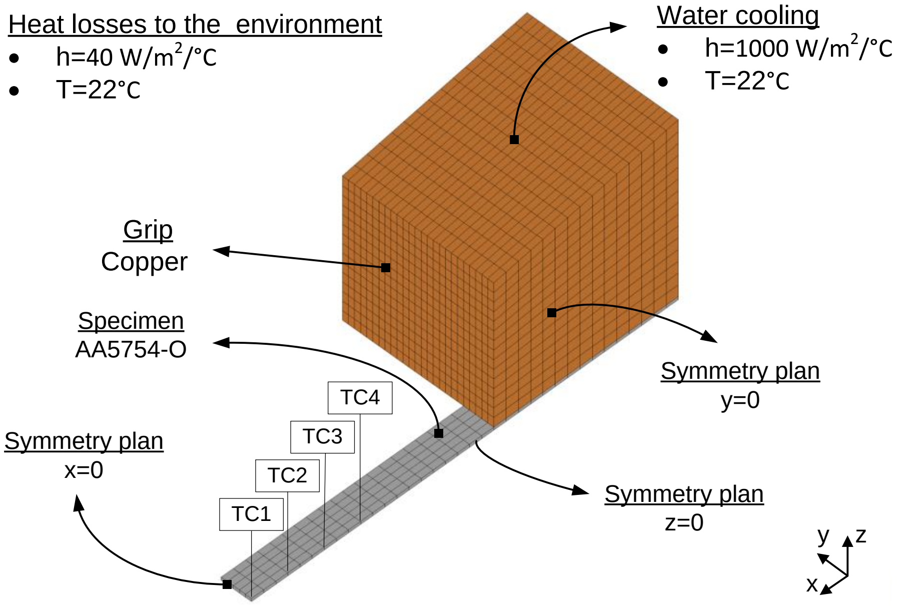

Figure 2. Tensile specimen and grips FE model used for the simulation of the Gleeble heating system (one eighth).

The distinction between the specimen and the grips was performed in the numerical model assigning different thermal properties to each region. The finite element mesh was generated in order to create nodes in the same positions of the four thermocouples used in the experimental set-up (see Figure 2). The Gleeble testing system heats the sheet by direct resistance using an electrical control scheme, which changes the applied current intensity to achieve a target temperature in the centre of the specimen, measured with a thermocouple (TC1 in Figure 1 (b)), for the time designated by the user [10]. The numerical modelling of the heat generated by electrical current is carried out in this study through an energy rate generation in the volume of the specimen (Eq. (9)), which is evaluated in each increment to try to guarantee a constant heating rate. The numerical temperature T^{c}, evaluated in the position of the thermocouple TC1, is compared with a pre-defined temperature T^{p}, in order to define the vector of heat generation using the predictor/corrector algorithm (Table 2). This pre-defined temperature T^{p} is calculated for every time instant, based on the prescribed heating rate.

The grips of the Gleeble system are water-cooled during the heating process. In the present study, the heat loss to the grips was modelled applying a high convection coefficient in the top surface of the grip, which is a procedure also adopted by Kardoulaki et al. [10]. The value of the convection coefficient used is 1000 W/m^2/ºC, with a temperature of 22ºC for the T_{∞} in Eq. (2). Additionally, the heat loss by convection to the environment was taken into account using a convection coefficient of 40 W/m^2/ºC and air temperature of 22ºC, as suggested in [22].

1. Initialize variables $\mathbf{T}_t = \mathbf{T}^{\text{initial}}$ and $t = 0s$.
2. **Prediction phase**

   2.1. **If** $\left\| T^{\text{p}} - T^{\text{c}} \right\| > 0$ **then**

   Calculate $\dot{q}_{t+\Delta t} = \rho c \dfrac{(T^{\text{p}} - T^{\text{c}})}{\Delta t}$

   End if

   2.2. Build and solve Eq. (16) for $\mathbf{T}_{t+\Delta t}$.
3. **Correction phase**

   3.1. **If** $\left\| T^{\text{p}} - T^{c} \right\| > tolerance$ **then**

   Calculate $\Delta\dot{q}^{i+1}_{t+\Delta t} = \rho c \dfrac{(T^{\text{p}} - T^{\text{c}})}{\Delta t}$

   Calculate $\dot{q}^{i+1}_{t+\Delta t} = \dot{q}^{i}_{t+\Delta t} + \Delta\dot{q}^{i+1}_{t+\Delta t}$

   End if

   3.2. Build and solve Eq. (21) for $\Delta\mathbf{T}^{i+1}_{t+\Delta t}$.

   3.3. If the equilibrium condition is not satisfied got to 3.1 for next iteration, otherwise proceed

   3.4. Next increment $t = t + \Delta t$, go to 2.

Table 2. Thermal properties of the specimen and grips materials [8], [14].

4. RESULTS AND DISCUSSION

The temperature distribution on the specimen, as well as on the grips, is presented in Figure 3. The water-cooling of the grips leads to a thermal gradient in the specimen caused by the heat removed from the grips. In fact, the temperature of the grips is approximately constant (22ºC) during the heating process of the specimen. The comparison between the experimental temperatures measured with the thermocouples and the numerical prediction is presented in Figure 4.

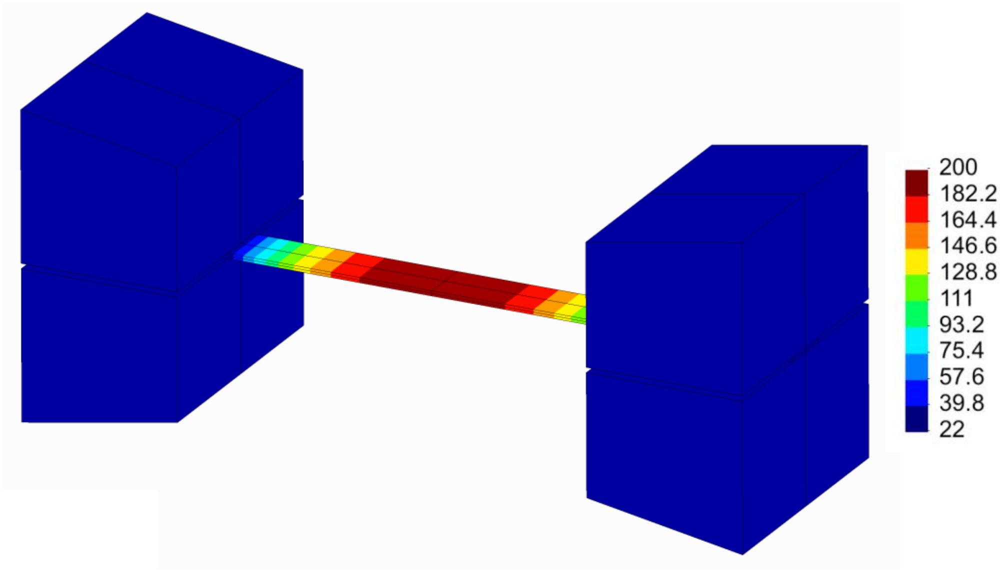

Figure 3. Temperature distribution in the specimen and grips for the heating process using a Gleeble system (complete model).

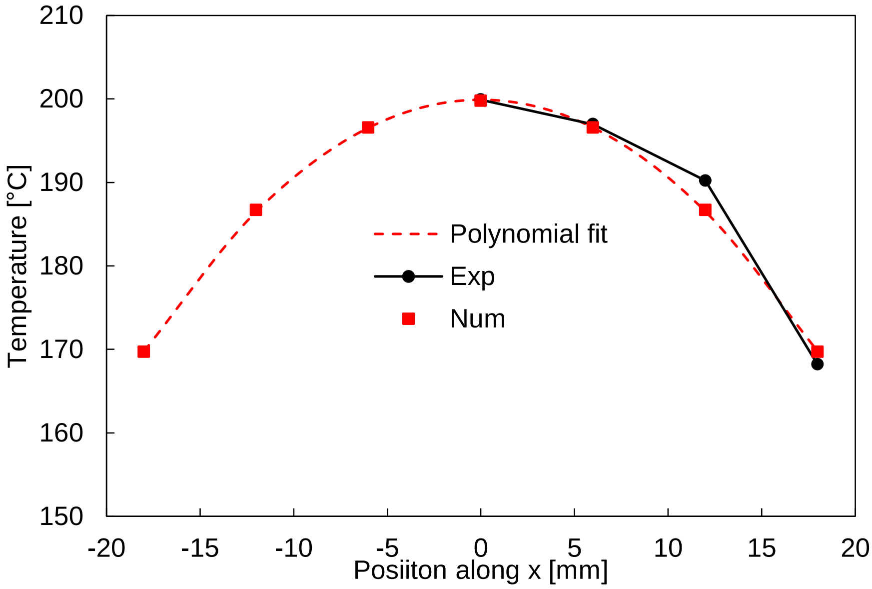

Figure 4. Comparison between experimental and numerical temperature distributions along the specimen length.

The finite element results are in good agreement with the experimental ones, particularly for the positions related with the thermocouples TC1 and TC2. Moreover, the numerical results can be exactly fitted by a quadratic equation, as shown in Figure 4, which is not observed in the experimental data. This difference can be caused by the influence of temperature in the material thermal properties, which was not taken into account in this model.

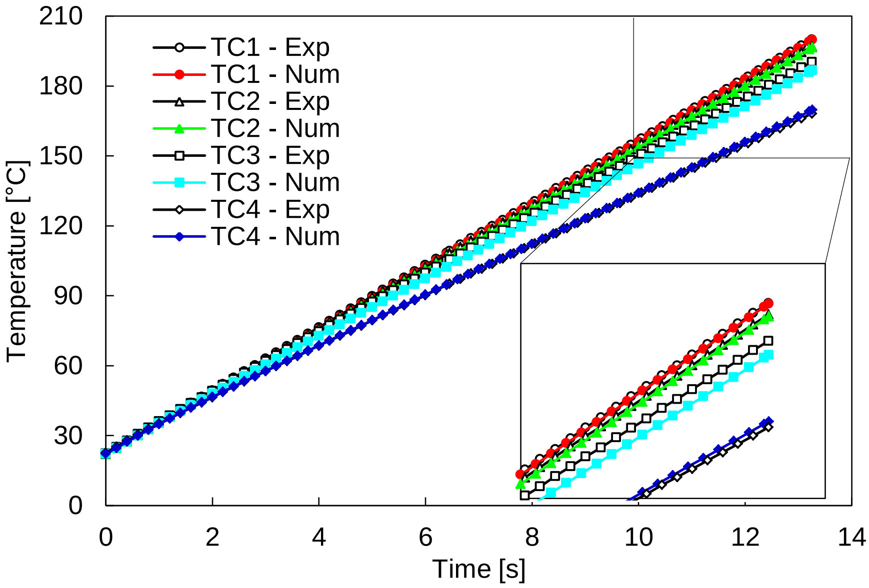

Figure 5. Temperature evolution in the thermocouples positions measured experimentally and calculated with the numerical model.

The transient thermal evolution of the specimen, recorded with the four thermocouples and predicted with the finite element model is presented in Figure 5. The temperature evolution is approximately linear for all points analysed, i.e. presents a constant heating rate. Besides, the numerical results are in good agreement with the experimental ones, in particular for the thermocouples TC1 and TC4. In order to highlight the difference between them, a detail view of the global evolution is also presented in Figure 5, for the last 3 seconds. The maximum difference between them is about 3.5ºC, which occurs in the thermocouple TC3 for the last instant (increment), as also shown in Figure 4.

5. CONCLUSIONS

This paper presents a transient finite element model to predict the temperature distribution/evolution on a tensile specimen heated by a Gleeble system. The algorithm used to evaluate the heat generation rate, physically produced by the direct resistance heating, was described. The results from the finite element model were compared with experimental results. Despite the several simplifications assumed in the model, the numerical results are in good agreement with the experimental ones, both in terms of temperature distribution and time evolution. Therefore, this model can be used in the development of inverse strategies for constitutive model parameters identification, based on experimental results obtained with the Gleeble device.

6. ACKNOWLEDGEMENTS

The authors gratefully acknowledge the financial support of the Portuguese Foundation for Science and Technology (FCT) under project PTDC/EMS-TEC/1805/2012 and by FEDER funds through the program COMPETE – Programa Operacional Factores de Competitividade, under the project CENTRO-07-0224-FEDER-002001 (MT4MOBI). The authors would like to thank Prof. A. Andrade-Campos for helpful contributes on the development of the finite element code presented in this work.

REFERENCES

[1] J. C. González Palencia, T. Furubayashi, and T. Nakata, “Energy use and CO2 emissions reduction potential in passenger car fleet using zero emission vehicles and lightweight materials,” *Energy*, vol. 48, no. 1, pp. 548–565, Dec. 2012.

[2] J. Hirsch, “Recent development in aluminium for automotive applications,” *Trans. Nonferrous Met. Soc. China*, vol. 24, no. 7, pp. 1995–2002, Jul. 2014.

[3] M. K. Kulekci, “Magnesium and its alloys applications in automotive industry,” *Int. J. Adv. Manuf. Technol.*, vol. 39, no. 9–10, pp. 851–865, Nov. 2007.

[4] S. Toros, F. Ozturk, and I. Kacar, “Review of warm forming of aluminum-magnesium alloys,” *J. Mater. Process. Technol.*, vol. 207, pp. 1–12, 2008.

[5] S. Kurukuri, A. H. van den Boogaard, A. Miroux, and B. Holmedal, “Warm forming simulation of Al–Mg sheet,” *J. Mater. Process. Technol.*, vol. 209, no. 15–16, pp. 5636–5645, Aug. 2009.

[6] M. Ghosh, A. Miroux, R. J. Werkhoven, P. J. Bolt, and L. A. I. Kestens, “Warm deep-drawing and post drawing analysis of two Al–Mg–Si alloys,” *J. Mater. Process. Technol.*, vol. 214, no. 4, pp. 756–766, Apr. 2014.

[7] N. Abedrabbo, F. Pourboghrat, and J. Carsley, “Forming of AA5182-O and AA5754-O at elevated temperatures using coupled thermo-mechanical finite element models,” *Int. J. Plast.*, vol. 23, no. 5, pp. 841–875, May 2007.

[8] H. Laurent, J. Coër, P. Y. Manach, M. C. Oliveira, and L. F. Menezes, “Experimental and numerical studies on the warm deep drawing of an Al–Mg alloy,” *Int. J. Mech. Sci.*, vol. 93, pp. 59–72, Apr. 2015.

[9] J. Coër, P. Y. Manach, H. Laurent, M. C. Oliveira, and L. F. Menezes, “Piobert–Lüders plateau and Portevin–Le Chatelier effect in an Al–Mg alloy in simple shear,” *Mech. Res. Commun.*, vol. 48, pp. 1–7, Mar. 2013.

[10] E. Kardoulaki, J. Lin, D. Balint, and D. Farrugia, “Investigation of the effects of thermal gradients present in Gleeble high-temperature tensile tests on the strain state for free cutting steel,” *J. Strain Anal. Eng. Des.*, vol. 49, no. 7, pp. 521–532, 2014.

[11] J. Coër, C. Bernard, H. Laurent, a. Andrade-Campos, and S. Thuillier, “The Effect of Temperature on Anisotropy Properties of an Aluminium Alloy,” *Exp. Mech.*, vol. 51, pp. 1185–1195, 2011.

[12] S. D. Norris and I. Wilson, “Application of 3D numerical modelling for thermal profile optimization on the Gleeble thermomechanical simulator,” *Model. Simul. Mater. Sci. Eng.*, vol. 7, pp. 297–309, 1999.

[13] S. G. R. Brown, J. D. James, and J. a Spittle, “A 3D numerical model of the temperature - time characteristics of specimens tested on a Gleeble thermomechanical simulator,” *Model. Simul. Mater. Sci. Eng.*, vol. 5, pp. 539–548, 1999.

[14] H. S. Kim and M. Koç, “Numerical investigations on springback characteristics of aluminum sheet metal alloys in warm forming conditions,” *J. Mater. Process. Technol.*, vol. 204, pp. 370–383, 2008.

[15] O. C. Zienkiewicz, R. L. Taylor, and J. Z. Zhu, *The Finite Element Method: its Basis and Fundamentals*. Elsevier, 2013.

[16] T. J. R. Hughes, *The finite element method: linear static and dynamic finite element analysis*. Courier Corporation, 2012.

[17] R. Madoliat and A. Ghasemi, “Inverse finite element formulations for transient heat conduction problems,” *Heat Mass Transf.*, vol. 44, pp. 569–577, 2008.

[18] M. Vaz Jr, “Simulação de Problemas de Acoplamento Termomecânico,” 2000.

[19] L. F. Menezes, D. M. Neto, M. C. Oliveira, and J. L. Alves, “Improving computational performance through HPC techniques: Case study using DD3IMP in-house code,” *AIP Conf. Proc.*, vol. 1353, pp. 1220–1225, 2011.

[20] A. Andrade-Campos, F. da Silva, and F. Teixeira-Dias, “Modelling and numerical analysis of heat treatments on aluminium parts,” *Int. J. Numer. Methods Eng.*, vol. 70, no. 5, pp. 582–609, 2007.

[21] H. L. Xing and a. Makinouchi, “FE modeling of thermo-elasto-plastic finite deformation and its application in sheet warm forming,” *Eng. Comput.*, vol. 19, pp. 392–410, 2002.

[22] H. Takuda, T. Morishita, T. Kinoshita, and N. Shirakawa, "Modelling of formula for flow stress of a magnesium alloy AZ31 sheet at elevated temperatures," *J. Mater. Process. Technol.*, vol. 164–165, pp. 1258–1262, 2005.